https://doi.org/10.5194/egusphere-2025-1149
Preprint. Discussion started: 25 March 2025

A data-driven wind-to-current response function and application to Ocean surface current estimates

Clément Ubelmann[1], J. Thomas Farrar[2], Bertrand Chapron[3], Lucile Gaultier[4], Laura Gómez-Navarro[5,6], Marie-Hélène Rio[7], and Gérald Dibarboure[8]

[1]Datlas, France
[2]Woods Hole Oceanographic Institution, MA, USA
[3]Ifremer, France
[4]Ocean Data Lab, France
[5]Utrecht University, The Netherlands
[6]IMEDEA (UIB-CSIC), Spain
[7]Esa-Esrin, Italy
[8]CNES, France

Correspondence: Clément Ubelmann (clement.ubelmann@datlas.fr)

Abstract. This study investigates modeling the wind-driven current using observed wind stress and an empirically estimated impulse response function for the wind-driven current response to wind forcing. Convolution of the data-driven impulse response function with the wind forcing gives an estimate of the wind-driven part of the current. We estimate this data-driven convolution operator using ERA5 reanalysis winds and observations of surface currents from drifting buoys. The response of the currents to wind forcing is expected to depend on the ocean mixed-layer depth and the turbulent viscosity profile with spatio-temporal variations, but we only consider seasonally-modulated and spatial variations in the training. Despite this crude approximation, the simplified response function explains a significant portion of the current variability. Indeed, when the function is applied to the ERA5 wind-stress, the surface current estimate compares reasonably well with independent observations (not used in the training).

A practical application is the release of new total surface current estimates such as the Globcurrent CMEMS MOB-TAC based on the same datasets, but here containing also the unsteady part of the wind driven currents (the inertial currents). The characteristics of the response function (amplitudes and phases) reveal interesting properties of the upper-ocean variability. The function shows some similarities to one derived theoretically from a simple 1-layer (slab) model, but also differences that highlight the value of fitting the function to the data without the use of an explicit dynamical model. This opens perspectives for studying some dependencies between subsurface variables and the response function, particularly interesting in the context of future spaceborne Doppler scatterometers such as ODYSEA, expected to provide simultaneous wind and current observations: this instrument could indirectly probe subsurface properties through the synoptically-observed response function.

https://doi.org/10.5194/egusphere-2025-1149
Preprint. Discussion started: 25 March 2025

1 Introduction

The transfer of momentum and energy across the air-sea interface provides sources of oceanic motions. Resulting upper ocean surface currents can then cover a wide range of temporal and spatial scales. A major component, called the geostrophic current, equilibrates the pressure gradient force and the Coriolis force. Pressure-gradients are currently well observed by satellite altimetry at spatial and temporal scales down to about 150km wavelength and 20-day periods (Ballarotta et al., 2019). Another important component, called the wind-driven current, is more directly related to atmospheric wind stress forcing. Over a range of depths not small compared to a ratio of the water velocity to the local Coriolis frequency, Coriolis effects become important. Direction and magnitude of the mean velocity field then vary with depth. A net transport in the upper ocean takes place, the Ekman transport, oscillatory in time with the inertial frequency, relative to and superimposed on the geostrophic motion. Wind-driven currents can reach large amplitudes, often exceeding the geostrophic current. Wind-driven currents are of interest for many scientific applications (e.g. Shrira and Almelah, 2020) and play an important role in the the ocean's energy budget (Flexas et al., 2019), but also for practical and societal applications, such as surface drift and accumulation of marine litter (Higgins et al., 2020; Cunningham et al., 2022). Besides seldom satellite synthetic aperture radar estimates (Chapron et al., 2005), total surface currents are not not directly observed at synoptic scale by satellite observations. However, estimates can be obtained from the knowledge of surface wind stress. In this study, we investigate the use of a data-driven response function. Despite the simplicity of the response function that excludes interactions with other components, it leads to an inverse linear problem, to further easily exploit the global drifter database to learn an effective ocean response to the wind forcing.

Some recent and extensive studies have been dedicated to theoretical aspects of the response of upper-ocean currents to wind forcing. In particular, Elipot and Gille (2009); Lilly and Elipot (2021) focused on the spectral transfer function between wind-stress and current, with extensive analysis of its dependencies with viscosity profiles in the ocean subsurface layers. We focus here on the closely related impulse response function, or just response function, that relates the ocean response to the wind forcing in the physical space. The impulse response function follows the Fourier transform of the spectral transfer function (Bendat and Piersol, 2010, p. 29, 26-27). Such a construction of the response function from real data and its applications to estimate the surface current at synoptic scales have not been fully explored yet. Some operational current products include an estimation of the Ekman component also based on a response function (GlobCurrent)[now operational in CMEMS, or the OSCAR dataset]. However, their response function is a single complex-scalar function limited to low-frequency estimates. As detailed in Lilly and Elipot (2021), the local response of the ocean to wind forcing at different frequencies can be described with a complex Fourier-space transfer function, equivalent to complex time-convolution response function in physical space.

In this study, we apply the convolution response-function concept to real observations and show the benefits of estimating it empirically. This is made possible because of the growing number of accumulated drifter data at high time-frequency (hourly outputs). The first practical application is the estimation of the wind-driven surface current at all times from the wind-stress reanalyses. Also, a more exploratory objective is to analyze whether the empirical response function constructed from the data alone can help us obtain new insights into ocean physics (like vertical mixing) and subsurface ocean properties (like mixed-layer depth). This is strongly motivated by the prospect of future spaceborne Doppler missions such as ODYSEA (Rodríguez

https://doi.org/10.5194/egusphere-2025-1149
Preprint. Discussion started: 25 March 2025

et al. (2019)) designed to observe simultaneously the surface wind and current at synoptic scale. Indeed, if the sparse drifter database can only provide spatio-temporally averaged response functions at best, the space-borne observation may allow a monitoring of the response function to probe subsurface characteristics.

The study is performed globally (70°S to 80°N). The time extension covers 2010-2020, a long period necessary to reach convergence in the response function estimate. Section 2 presents all the datasets. Section 3 presents the motivation behind the determination of the response function. Section 4 covers the application to surface current estimates, including the validation, and section 5 explores some characteristics of the response function and its characteristics with respect to subsurface dynamics.

2 Datasets : ERA5 wind stress, surface drifter velocities and altimeter-derived geostrophic current

Three datasets are considered in this study: the surface drifter velocities (sparse total current observations), the geostrophic current and the Ocean surface wind-stress, from years 2010 to 2020.

The surface drifter velocities have been extracted from the global drifter database (Elipot et al. (2016)). Only the 'drogued' drifters are considered in the main experiment, representative of the current at 15m depth which is the focus of this study. The velocity variables (pre-processed from the positions) at hourly frequency are used. Both Argo and GPS data are used to allow the 10-year extension of the study, although the GPS data are more accurate and fairly dominant after 2015.

The geostrophic velocity dataset from CMEMS (Taburet et al. (2019)), derived from muti-satellite altimetry maps, have been co-located at all drifters hourly positions. A linear interpolation scheme is used between the daily 1/4° grid and the drifters. These estimates are used to substract from the total velocity measured by the drifters, in order to isolate the ageostrophic component representative of the u variable in the equations presented next section.

The ERA5 surface wind-stress product at hourly resolution on a 0.25° spatial grid (Hersbach (2018)) is used as the forcing term described in the following. The data were provided by the Copernicus service.

Figure 1 illustrates the main datasets, during an event where a strong atmospheric front resolved by ERA5 triggers inertial currents captured by a drifter. On the upper-right panel, the drifter features clear oscillations after the passage of the atmospheric front. This gives some confidence on the reliability of the datasets to explore the unsteady-Ekman response.

3 The data-driven response function

3.1 The rationale for a response function

The equations governing the horizontal currents in the upper ocean can be written approximately as (e.g., Gill, 1982, p. 320),

$$\frac{\partial u}{\partial t} - fv = \frac{1}{\rho}\left(-\frac{\partial p}{\partial x} + \frac{\partial \tau^x}{\partial z}\right) \tag{1}$$

$$\frac{\partial v}{\partial t} + fu = \frac{1}{\rho}\left(-\frac{\partial p}{\partial y} + \frac{\partial \tau^y}{\partial z}\right) \tag{2}$$

https://doi.org/10.5194/egusphere-2025-1149
Preprint. Discussion started: 25 March 2025

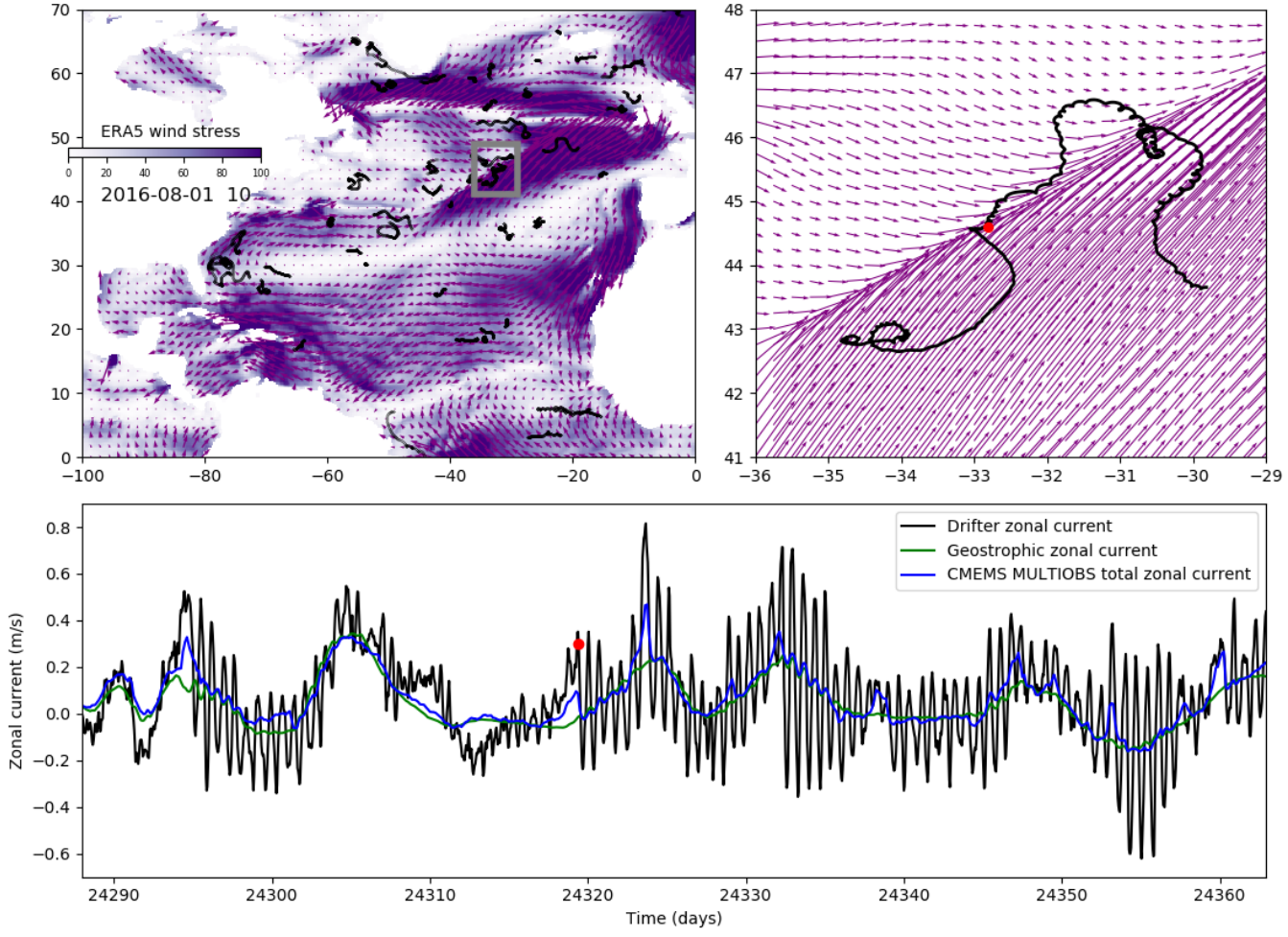

Figure 1. Illustration of the main datasets used in the study. Upper-left panel : a snapshot of the ERA5 wind stress superimposed with the ensemble of drifter positions over +/- 20 days. Upper right: zoom of the first panel highlighting the presence of a drifter near a strong atmospheric front (the red dot is the position at the present time). Lower panel: time series of the zonal velocities derived from the drifter trajectory (black), with a colocation of the geostrophy from altimetry (green) with added CMEMS Ekman estimate (blue). showing that inertial oscillations are triggered after the crossing of the atmospheric front.

where $\mathbf{u} = (u, v)$ is the horizontal current vector, f is the local Coriolis parameter (or inertial frequency), ρ is the density, p is the pressure and $\tau = (\tau^x, \tau^y)$ is the horizontal stress vector. (Horizontal advection terms have been neglected.) Assuming there is no nonlinear dependence of τ or p on $\mathbf{u}$, these equations are linear.

We are interested in how the upper ocean responds to wind forcing. We can conceptually separate the velocity vector $\mathbf{u}_{total}$ into a pressure-driven component $\mathbf{u}_g$ and a stress-driven component (or unsteady-Ekman component) $\mathbf{u}_e$, which is governed

https://doi.org/10.5194/egusphere-2025-1149
Preprint. Discussion started: 25 March 2025

by

$$\frac{\partial u_e}{\partial t} - f v_e = \frac{1}{\rho}\frac{\partial \tau^x}{\partial z} \tag{3}$$

$$\frac{\partial v_e}{\partial t} + f u_e = \frac{1}{\rho}\frac{\partial \tau^y}{\partial z} \tag{4}$$

To relate the wind-driven current, $\mathbf{u}_e$, to the wind-stress forcing (or the value of τ) at the surface, τ_0, an impulse response formulation writes

$$\mathbf{u}_e(x,y,t) = \int_{-T}^{0} G(t')\tau_0(t+t')dt' \tag{5}$$

where G is a complex function of time lag t', and the integral from $-T$ to 0 expresses the fact that the output can only depend on the time-history of the wind stress forcing. We assume the unsteady-Ekman current only affected by this wind history over a limited time, and T is set to be about a week.

The inversion problem is to retrieve G, given drifter observations of $\mathbf{u}_e$ (approximated by the velocity derived from the position minus the geostrophic current from altimetry, as illustrated on the bottom panel of Figure 2), and from the Eulerian history of ERA5 wind stress at each drifter location (upper panel of Figure 2). These two series, here shown for 75 days for a specific drifter, are generated using all drifters (except for a few, withheld for validation) in the studt area over the 10 years.

Note, additional signals are obviously present, combining imperfect geostrophy estimates, ageostrophic motions not resolved by altimetry, errors from the drifter measurements, etc... We assume these additional signals are uncorrelated with the wind-driven motions we aim to retrieve.

Vertically integrating Eqns 3-4 from the surface to some depth H, the vertically averaged velocity $(\bar{u}_e, \bar{v}_e)$ are:

$$\frac{\partial \bar{u}_e}{\partial t} - f \bar{v}_e = \frac{\tau_0^x - \tau_H^x}{\rho H} \tag{6}$$

$$\frac{\partial \bar{v}_e}{\partial t} + f \bar{u}_e = \frac{\tau_0^y - \tau_H^y}{\rho H} \tag{7}$$

where (τ_H^x, τ_H^y) correspond to turbulent stress at depth H. These equations are one version of the "slab model", commonly used to model mixed-layer inertial currents (e.g., Plueddemann and Farrar, 2006; Alford, 2020). Considering (τ_H^x, τ_H^y), linearly proportional to the layer-averaged velocity, $(\tau_H^x, \tau_H^y) = r\rho H(\bar{u}_e, \bar{v}_e)$, the well-known "damped slab" model of the mixed layer is recovered (e.g., D'Asaro, 1985):

$$\frac{\partial \bar{u}_e}{\partial t} - f \bar{v}_e = \frac{\tau_0^x}{\rho H} - r\bar{u}_e \tag{8}$$

$$\frac{\partial \bar{v}_e}{\partial t} + f \bar{u}_e = \frac{\tau_0^y}{\rho H} - r\bar{v}_e \tag{9}$$

Writing the vector components in complex notation ($Z \equiv \bar{u}_e + i\bar{v}_e$ and $T \equiv \bar{\tau}_0^x + i\bar{\tau}_0^y$), the damped slab model is given by

$$\frac{\partial Z}{\partial t} + (r + if)Z = \frac{T}{H} \tag{10}$$

which has the impulse response function

$$G(t) = \frac{e^{-rt}}{H} e^{-ift}. \tag{11}$$

https://doi.org/10.5194/egusphere-2025-1149
Preprint. Discussion started: 25 March 2025

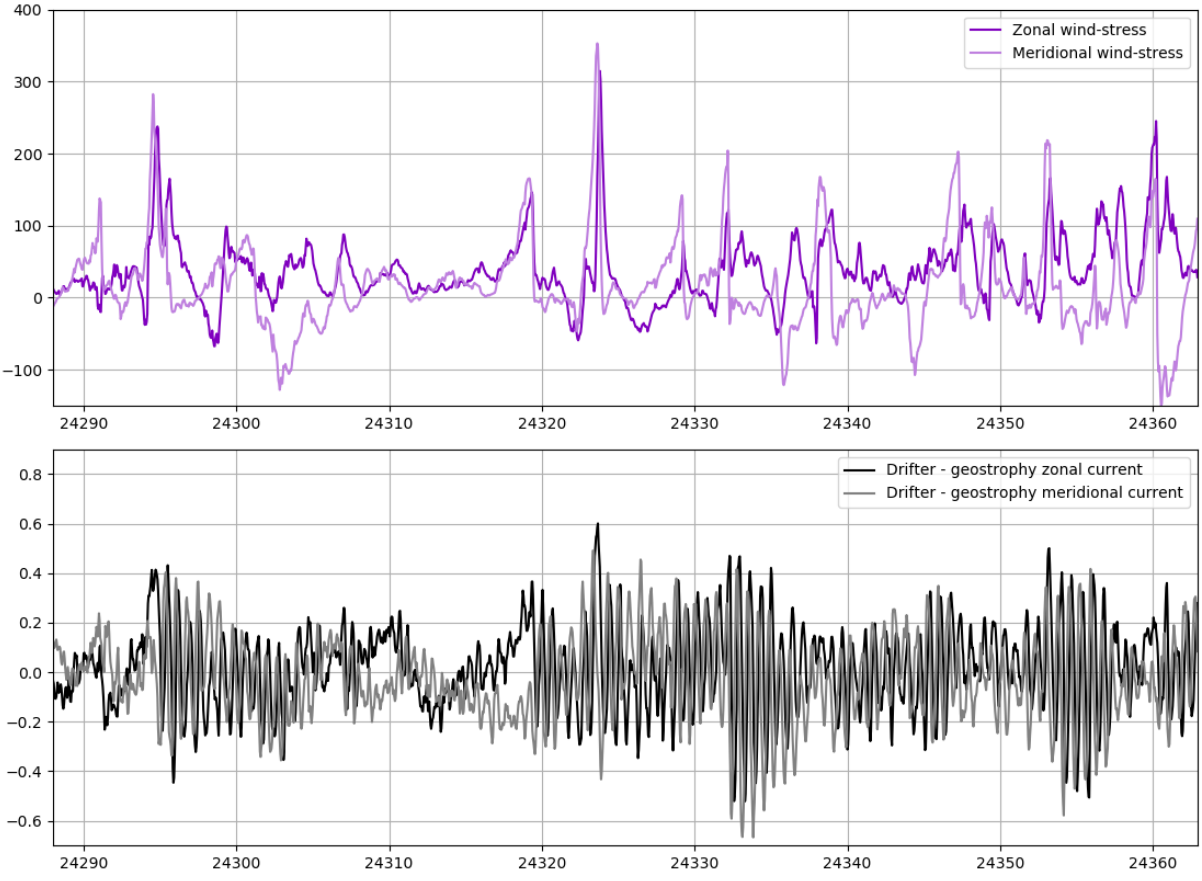

Figure 2. Example of Lagrangian time series of the ERA5 wind stress (zonal and meridional components) co-located at a drifter position (upper panel) and time series of the drifter-derived ageostrophic velocity (lower panel).

$G(t)$ is defined for $t = 0$ to $t = \infty$. For the damped slab model, the impulse response function oscillates at frequency f with an amplitude that is inversely proportional to mixed-layer depth, H, and decays with time with an e-folding decay timescale of $1/r$. One can "run" the damped slab model convolving $G(t)$ with an observed wind stress T $(\bar{\tau}_0^x + i\bar{\tau}_0^y)$.

One *could* simply fit the parameters in Eqns 10 or 11 to the data to make a model of the inertial response. As noted by Plueddemann and Farrar (2006), Alford (2020), and others, the damping of mixed-layer inertial motions involves various kinds of physics (e.g., turbulent momentum transport, wave radiation stresses) acting on different timescales, and so a single damping parameter cannot adequately represent all of the processes removing momentum and energy from the near-surface ocean. Thus, it is preferable to estimate G in Eqn 5 without having to rely on the approximations beyond those in Eqns 3-4.

https://doi.org/10.5194/egusphere-2025-1149
Preprint. Discussion started: 25 March 2025

3.2 The degrees of freedom for G

Over the oceans, very different conditions of stratification and mixed layer depth in particular can be found, so we cannot expect the G response function to be uniform. Nevertheless, the amount of drifter data is limited and to avoid over-fitting issues, we cannot let G vary totally freely. In order to have a good compromise, we defined a reduced space where a G function can vary with latitude, and seasonally. If η is a parameter vector in this reduced space, G is decomposed by a series of linear operators under the form:

$$\mathbf{G}(\mathbf{x},\mathbf{y},\mathbf{t},\mathbf{t}') = \mathbf{\Gamma}(\mathbf{t}')\mathbf{S}(\mathbf{t})\mathbf{L}(\mathbf{x},\mathbf{y})\eta \tag{12}$$

where $\mathbf{L}$ is a bi-linear spatial interpolator transforming the ensemble of values for η in the parameter space into a local set of parameters at location (x, y). Then, the operator $S(t)$ applies the seasonality reducing into a subset of parameters at the time of the year (in practice, one constant, one sine and one cosine functions are defined at the annual-frequency). Finally, Γ converts the subset of parameters into the response function value at relative time t'.

3.3 Resolution of the inverse problem to fit G

The series of operators transforming η into the local (spatially and seasonally) convolution function are linear. The convolution operator is also linear. Therefore, the wind-driven current vector u_e at the difter location can be written as:

$$\mathbf{u_e} = \mathbf{M}\eta + \epsilon \tag{13}$$

where $\mathbf{M}$ is a linear operator including the successive construction of G and the convolution operation with the wind-stress, all linear with respect to η . This inverse problem can be solved by minimizing the following cost function :

$$\mathbf{J} = \|\mathbf{M}\eta - \mathbf{u_{obs}}\|^{\mathbf{2}} \tag{14}$$

We used a conjugate gradient descent involving iterative computations of the gradient of the cost function:

$$\nabla\mathbf{J} = \frac{\mathbf{1}}{\mathbf{2}}\mathbf{M^T}(\mathbf{M}\eta - \mathbf{u_{obs}}) \tag{15}$$

In practice, the adjoint operator $\mathbf{M^T}$ is applied from the adjoint of the linear operations in Eq. 12 and from the adjoint of the convolution Eq. 5. For the problem considered, the convergence was reached after about a hundred iterations.

4 Application to surface current estimates and validation

A direct application of the response function fitted from the drifters is an estimation of the wind-driven current over a continuous time/space grid as it is for the input ERA5 wind-stress from the reanalysis. This was performed over the 10-year of study on the 0.25° resolution grid of the ERA5 input data. The upper panels of figure 3 show snapshots of the current obtained with

https://doi.org/10.5194/egusphere-2025-1149
Preprint. Discussion started: 25 March 2025

the response function (right, called the WOC estimates hereafter) compared with the current form the CMEMS Ekman model (left). On the right, higher amplitudes are reached, with an imprint of oscillatory patterns after the passage of the atmospheric front near 45°N, 40°E. The lower panel shows these estimations as a function of time in red and blue respectively (with added geostrophy represented in green) co-located with a drifter in black (this drifter was excluded from the training).

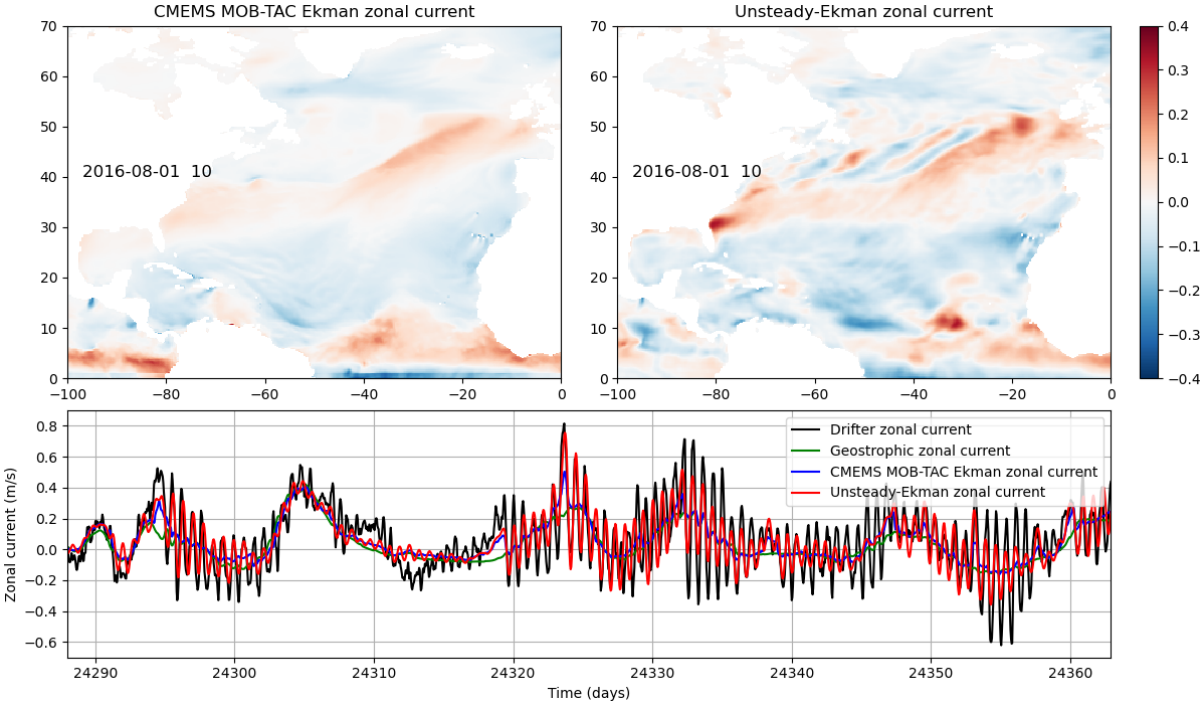

Figure 3. Illustrations of the wind-driven zonal current from the CMEMS MOB-TAC (upper left) and from the WOC response-function approach (upper right). Bottom : time series from the response-function approcah (red line) colocated at in independant drifter position, after addition of an estimate of the Geostrophic zonal current (green line). The estimated current captures many of the details of the zonal current observed independently by the drifter (black line).

A significant part of the observed inertial oscillations are captured by the WOC response function estimation with a phase that seems quite accurate in this example (we picked a case with particularly intense inertial oscillation for the illustration). Not surprisingly, the amplitude is attenuated since the estimation is designed to minimize root mean square, and there is a significant part of unresolved signal. The latter may be explained by two main sources: the imperfect wind and the locally specific subsurface turbulent viscosity conditions not captured by the climatological variations of G (mixed layer or more generally the density profile). Additional sources may also be the results of interaction between the wind-driven current and the mesoscales (e.g. Young and Jelloul (1997)) or simply the presence of submesoscale currents.

Some quantitative diagnostics can be applied to the ensemble of independent drifters to assess the reconstruction skills more quantitatively and in all situations (not only during strong wind events). On the top panel of figure 4, we represent in

https://doi.org/10.5194/egusphere-2025-1149
Preprint. Discussion started: 25 March 2025

black the power time-frequency spectrum of the observed drifter current between 1000 hours and 2 hours (in the clockwise direction on the left and counter-clockwise on the right) averaged over the oceans between 40°N and 50°N. The thick colored lines represent the resolved energy by the different estimations: geostrophic in green, Globcurrent/CMEMS (including Ekman) estimation in blue, and the WOC estimation of wind-driven current including the inertial component, in red. As anticipated by the resolved oscillations on Figure 3, the red spectrum features a clear peak at the inertial frequency (near 18 hours at these latitudes in the clockwise panel), of about 40% of the energy seen by the drifters (black). We note that the sub-inertial band between 100 hours and 18 hours has also gained some energy compared to the Globcurrent/CMEMS product. However, it is interesting to note that the counter-clockwise spectrum is very similar to Globcurrent/CMEMS, and only slightly above the spectrum of geostrophic current. The second peak at 12h frequency, present in both clockwise and counter-clockwise spectra of the drifter, is not resolved by the reconstructions. It corresponds to tidal currents (barotopic near the continental shelves, and mostly baroclinic in open-ocean) not resolved by design in any of the estimates.

The levels of energy do not tell us anything about whether the reconstructions have accurate phases. To examine the accuracy of the phase, we also computed the spectrum of the observations minus the spectrum of the difference between the estimation and the observations. This diagnostic shows how much of the observation variance is explained by the estimation (the thin colored lines). We note that, overall, the levels are similar to the spectra of the estimations suggesting that the phases of the resolved signals are correct. Except for the Globcurrent/CMEMS estimation in the inertial band: the energy is very low (no inertial peak), but the explained variance is much above suggesting that the phases are correct although the energy is damped. This is consistent with what we can observe on Figure 3: the blue curve tends to follow the first oscillation of NIO events, but with a strong attenuation and only after the wind impulses (by design of the non-convolutive response function).

The resolved variances are also represented in percentages on the bottom-left panel. Not surprisingly, the WOC with its inertial component captures more of the energy in the near-inertial band (30%-40% more), confirming the qualitative results from Figure 3. Also, at lower frequencies, the skill scores are similar between the Globcurrent/CMEMS and WOC, which is consistent. These estimations provide an additional gain of about 10% above the geostrophic current only. However, there is still 40% to 60% current missing in this sub-inertial to inertial frequency range.

Regarding the counter-clockwise scores, the percentages confirm that the Globcurrent/CMEMS and WOC are fairly similar, with slight improvements from geostrophy.

The same diagnostics have been performed in the tropical region between 5°-10°N as shown on Figure 5. In this region the inertial frequency gets shifted toward low-frequencies becoming hard to distinguish from the other dynamics. Nevertheless, the peak is clear (spread between 200 and 50 hours) and the reconstruction skills are comparable to that of the higher latitudes. We note that the WOC spectrum drops more rapidly in the super-inertial band, but where none of the products have significant scores anyway (the phases are not consistent with observations in the super-inertial band).

Regarding the counter-clockwise scores, the results are also similar to that of mid-latitudes (with overall less contribution from Altimetry as expected in the tropics).

A graphic of the explained variances as a function of latitude is shown in Figure 6. In this diagnostic, all frequencies are considered, but the view along the latitude dimension, separately for the zonal and meridional current, is instructive. First,

https://doi.org/10.5194/egusphere-2025-1149
Preprint. Discussion started: 25 March 2025

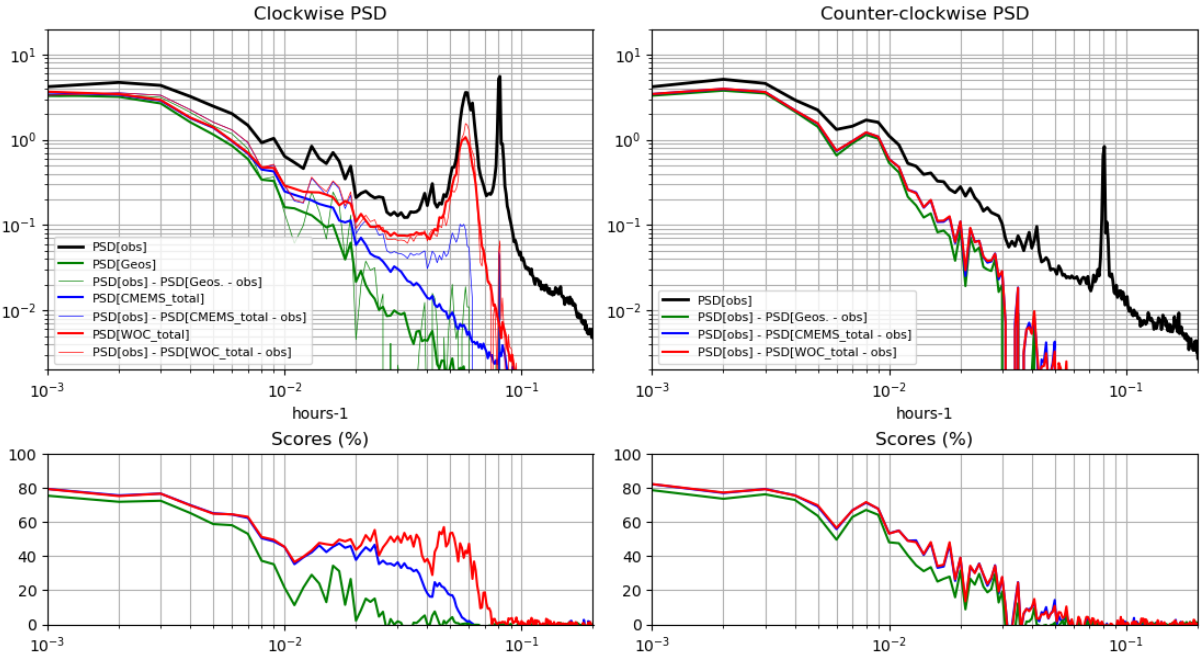

Figure 4. Upper-left panel: power spectral density (in the clockwise time-frequency domain between 1000 hours and 2 hours) of the drogued-drifter current observations in the 40°N to 50°N latitude range, in black. The thick-colored curves represent the power spectral densities of the various estimates (geostrophic, GlobCurrent/CMEMS and WOC impulse function estimates in green, blue, and red, respectively). The thin-colored curves represent the spectrum of the observations minus the spectra of the difference between the estimation and the observations. Upper-right panel : same, in the counter-clockwise direction. Lower panels : ratio between the thin-colored curves and the black curve of the upper panesl, multiplied by 100, representing the percentages of reconstruction (explained variance).

we note the strong zonal current variability of the Equatorial currents seen by the drifters. Here, the altimetry contribution owes to the Lagerloef et al. (1999) derivation implemented in the CMEMS geostrophic current product near the Equator, explaining about 1/3 of the variability. This derivation does not provide accurate currents in the meridional direction for which the altimetry contribution is zero near the Equator (right panel). The Globcurrent/CMEMS and WOC estimation provide improvements, more pronounced on the zonal component. At higher latitudes, the zonal and meridional components show similar explained variances for the different estimations. Overall, if we look at the globally-averaged values from Figure 7, geostrophy explains 40% of the surface current variability, and the WOC estimation brings an additional 12% to 14% for the zonal and meridional components respectively. This is significantly above the Globcurrent/CMEMS that brings 6% to 9% for the zonal and meridional components respectively. This may appear small, but the inertial currents are intermittent and therefore the contribution is certainly much higher at times, particularly just after a wind event that triggers inertial oscillations. Nevertheless, there is still a large part of unexplained surface current in the drifters (gray areas on the Figure) leaving some room for further scientific investigations that will be discussed in conclusions.

https://doi.org/10.5194/egusphere-2025-1149
Preprint. Discussion started: 25 March 2025

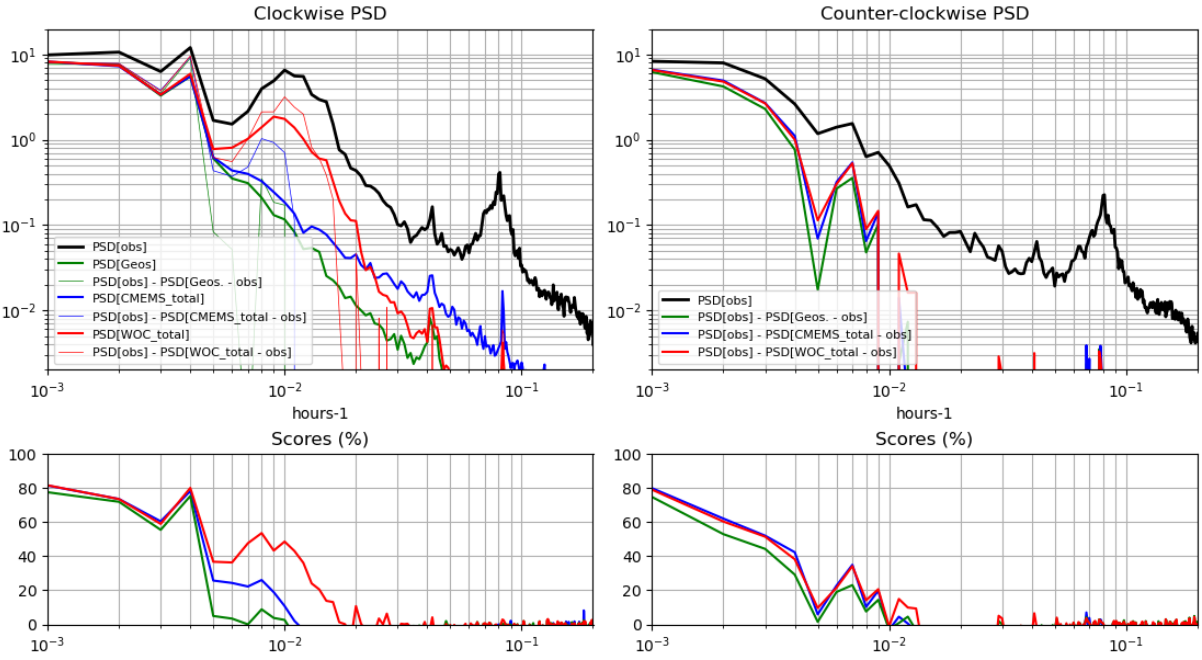

Figure 5. Same as Figure 4, averaged between 5°N and 10°N.

5 Characteristics of the response function

The response function defined as a bivariate (in the complex 2D plane) convolution over a few days revealed to be efficient in capturing an additional part of the observed surface current, in particular in the inertial band. It is now interesting to analyze the features of the empirically determined response function, and in particular its potential variations with the season and the latitude.

Figure 9 represents the response function as a function of time, defined between -1 day and +8 days at different latitudes and seasons, and separately for the 15 m drogue drifters (blue) and the 0 m undrogue drifters (red).

First, the values of G are close to zero for negative t', suggesting that the future wind stress is not (significantly) related to the present current, which is consistent with the fact that ocean currents respond to the wind forcing, rather than the ocean currents forcing the wind. (We tested a centered window between -8 days and +8 days and also obtained values of G close to zero for negative t'.) However, ocean feedbacks to the atmosphere obviously exist (e.g., Renault et al., 2016), but this is not detected in the linear framework of the response function. Then, for positive t', the clear oscillations of G indicate the impact of the wind history over a few days. These oscillations are close to the inertial frequency (varying with latitude) as expected by Eq. 11, with an observed decay. Through the convolution, these oscillations act in triggering the inertial oscillation in response to an atmospheric forcing that contains some energy at the Coriolis frequency.

The black curve represents fit for the slab layer response function of Eq. 11. Beyond 12h lag, the slab model, the 15m-drogued-drifter response function, and the undrogued-drifter response functions all show similar behavior. The effect of the

https://doi.org/10.5194/egusphere-2025-1149
Preprint. Discussion started: 25 March 2025

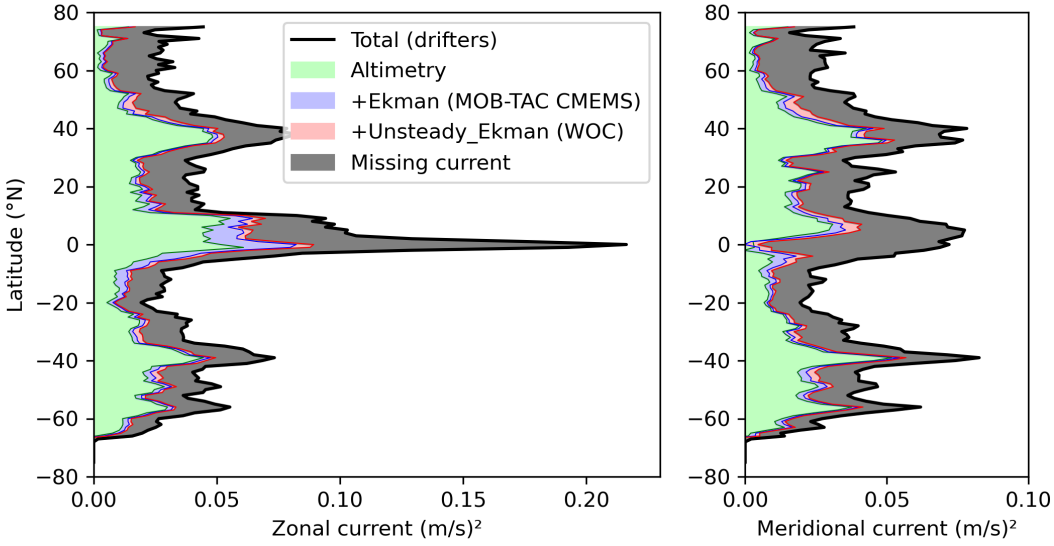

Figure 6. Variance of the surface current (zonal component on the left, meridional on the right) as a function of latitude averaged globaly for the drifter database between 2017 and 2020. The black line is for the total current derived from the drifters. The green, blue and red lines are the variance reduction after applying the Geostrophy from CMEMS, the Globcurrent/CMEMS (geostrophy+Ekman) the WOC estimates (geostrophy+Unsteady_Ekman)

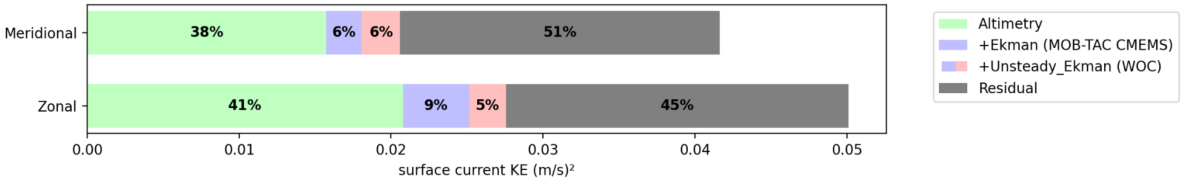

Figure 7. Same as Figure 6 averaged globally

seasons at high latitudes is very clear. At 55°N in the winter, the inertia is twice that of the summer (the thickness of equivalent slab is doubled). In the tropics, the seasonality is much less pronounced as expected. We note that the decay rate is quite similar between winter and summer, and is slightly longer at high latitudes than in the tropics. The decay is likely the combination of two effects at least. One is the actual attenuation of the NIOs in response to a wind impulse, and the second is an additional apparent attenuation due to local modifications of the inertia frequency in response to relative vorticity for instance or other factors impacting the phase. Since the response function relies on a least-squares fit, these uncertainties tend to attenuate the actual response, especially at large negative time values.

Beyond the similarities with the slab response, what is particularly interesting are the clear differences in the first few hours of the response function, for both the drogued and undrogued drifters in a different manner. The values at short time lags can

https://doi.org/10.5194/egusphere-2025-1149
Preprint. Discussion started: 25 March 2025

be interpreted as the result of dynamics occurring right after the wind impulses (typically after the crossing of an atmospheric front). In the following, we speculate on possible interpretations for the observed differences. A first striking feature is the peak of the real part of the function at zero time-lag for the undrogued drifters. This indicates a direct velocity triggered instantaneously in the wind direction (as the imaginary part remains close to zero). Several effects may explain this peak. A first one is wind-slippage to which undrogued drifters are known to be affected (e.g. Rio et al. (2014)). The response is indeed immediate to the wind forcing and along its direction. A second one is the Stokes drift from the wind-waves that should also respond rapidly (although not instantaneously) in the wind direction. However, we do not have a clear explanation why the peak seems less pronounced at low-latitudes.

The 15m depth drogued drifters have also interesting departures from the slab in the first few hours. In particular during the winter at high-latitudes. One hypothesis is the presence of temporary re-stratified layers over the very deep mixed layer. This temporary layer would respond to the wind front as a thinner layer in the first hours until the strong mixing (due to the increased wind) transforms the deep mixed layer depth as an active mixing layer, therefore behaving like a slab. In the tropics, we seem to observe an opposite effect at 15m depth with the blue curve reduced in the first 12 hours. This actually might be the result of the same process, but for thinner temporary layers, therefore above the 15m drogue, then destroyed after strong wind impulses.

Although the causes are speculative, this suggests that specific dynamical regimes, fairly different from the slab, are also involved and play a role on the surface current response to wind stress.

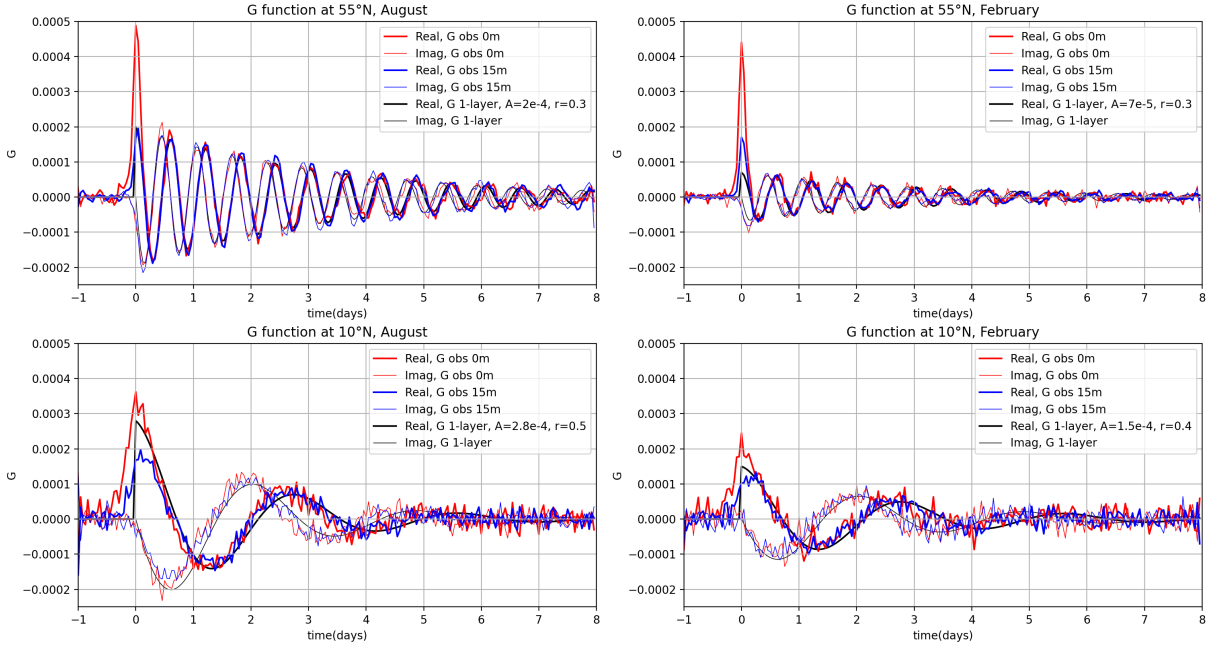

Figure 8. Upper-left panel : mean G function in August at latitude 50°N, represented as a function of the t' interval, for the real (plain line) and imaginary parts (dotted line). Upper-right panel : same function in February. Lower panels : same as upper panels, averaged at 10°N.

https://doi.org/10.5194/egusphere-2025-1149
Preprint. Discussion started: 25 March 2025

Another representation of the same response functions is proposed on Figure 8 along the real and imaginary axes. Here, we convolve the response function with a step-function for the wind. This step function, represented by the green arrow along the imaginary axis, is zero for negative time and unitary for positive time. The results, here called the equivalent step-response functions as represented on the figure, highlight additional features. In particular, the low-frequency response, ending at a given angle to the right of the wind (here in the northern hemisphere) can be clearly assessed both the surface and drogued drifters. The slab-derived step-response functions have constrained angles in the 70°-80° range for the typical values of damping, which is more than what is fitted for the undrogued and drogued drifters. (As is well known, the form of the damping used in the slab model causes the Ekman transport to be slightly less than 90° to the right of the wind.) This again illustrates well the differences and the interest of considering these response function beyond a pure slab dynamic.

6 Conclusions and perspectives

This study demonstrated that a purely empirical relation between wind forcing and the wind-driven surface current (Ekman and inertial currents) can be easily learned from the drifters to provide surface current estimates based on ERA5 wind stress. It provides a potential step forward to the operational Globcurrent MOB-TAC CMEMS surface current, based on the same datasets but here exploiting higher frequencies through estimation of an impulse response function. This is now possible globally because of the recent accumulation of high-quality drifter data at high-frequency. The surface current estimates have been successfully validated with independent observations. Although the gain of explained variance remains overall of 10% compared with MOB-TAC CMEMS, the gain during intermittent near inertial oscillation events is certainly much higher.

The analysis of the response function learned from the drifters may also yield new insights into the physics. Indeed, we found that the similarities with a slab model response are not always true especially in the first few hours of the response. Speculative causes have been discussed, in relation with the existence of temporary layers. The longer term (>12h) response is nonetheless similar with a slab response, for both undrogued and 15m-drogued drifters, and with amplitudes clearly related with the seasons out of the tropics (the thickness of the slab being larger in the winter season). This computation of the response function opens the door for considering further dependencies beyond the seasons and location to better understand the physical processes in the first layers in response to the wind. For instance, additional parameters such as the subsurface density profile or sea state may be introduced as parameters in the empirical computation of the response function.

These more complex dependencies probably partly explain why a large part of the signal is still unresolved when compared to independent observations. We expect that a lot of progress can be made by considering additional datasets that contain additional information on local sub-surface properties, which could also allow new insights into the physics of the subsurface processes. (Inadequacies of the high-frequency winds may also explain another part the remaining signal, as supported by Klenz et al. (2022).) We could potentially learn a great deal more about the physical processes in upper ocean from global, coincident measurements of ocean vector winds and ocean surface currents that could be measured from satellites (e.g., Rodríguez et al., 2019) by using a data-driven approach to examine the relationship between the two quantities.

https://doi.org/10.5194/egusphere-2025-1149
Preprint. Discussion started: 25 March 2025

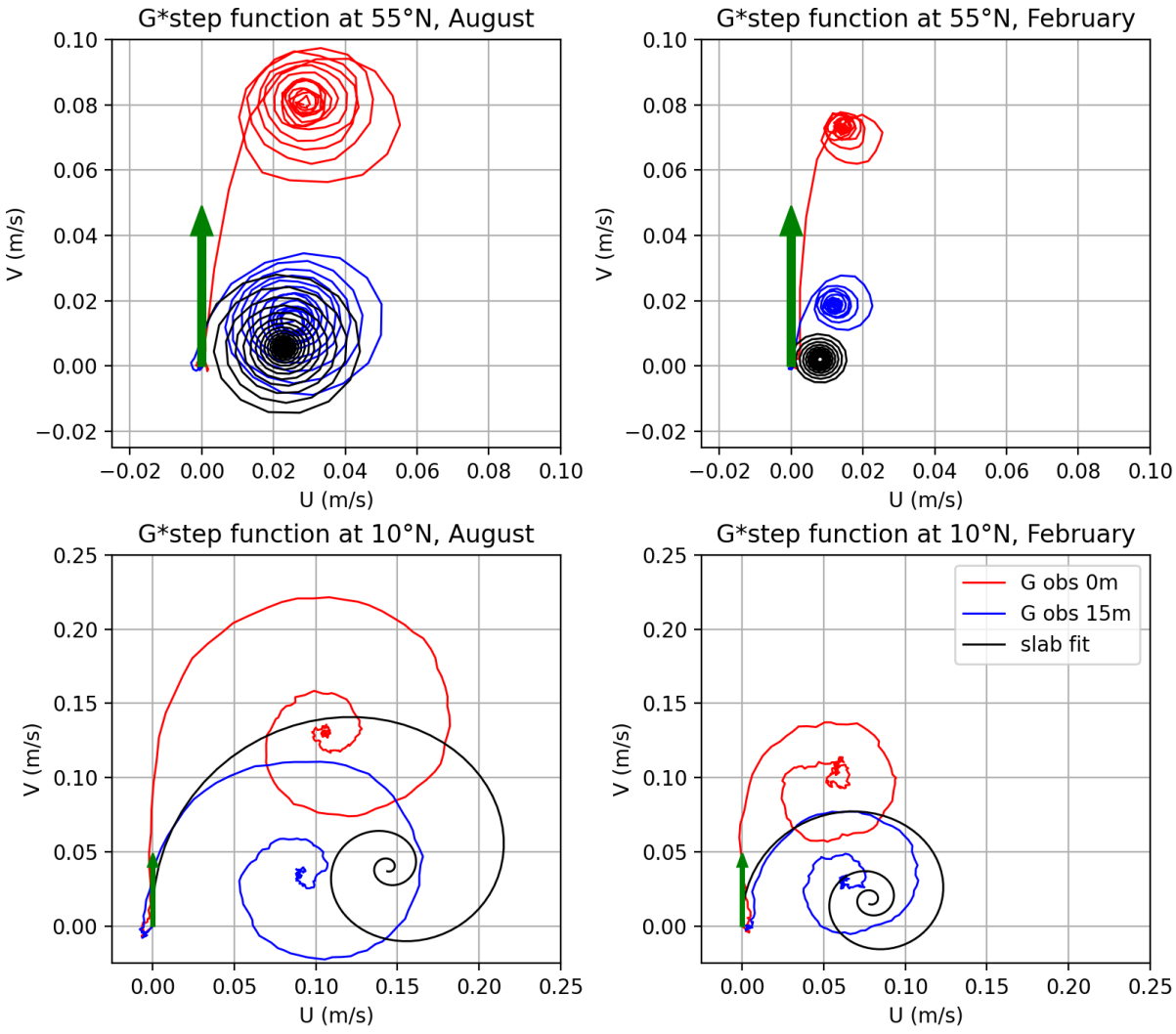

Figure 9. Integration of the response function with a unitary-step function of the wind represented by the green arrows. The result, called step-response functions, are represented in the (Real,Imaginary) plane by the red, blue and black lines for the undrogued drifters, drogued drifters and slab respectively.

Data availability. The dataset of surface current generated in this study is available on the World Ocean Circulation ESA project website: https://www.worldoceancirculation.org/

Competing interests. The authors declare that no competing interests are present.

https://doi.org/10.5194/egusphere-2025-1149
Preprint. Discussion started: 25 March 2025

Acknowledgements. This research was funded by the European Space Agency through the World Ocean Current project (ESA Contract No. 4000130730/20/I-NB) with complement from the Centre National d'Etudes Spatiales (CNES Contract No. 230376-00 ODYSEA Phase A support) . JTF was supported by the US National Aeronautics and Space Administration (Contract 80GSFC24CA067), via a subaward from the University of California San Diego to the Woods Hole Oceanographic Institution.

https://doi.org/10.5194/egusphere-2025-1149
Preprint. Discussion started: 25 March 2025

References

Alford, M. H.: Revisiting Near-Inertial Wind Work: Slab Models, Relative Stress, and Mixed Layer Deepening, Journal of Physical Oceanography, 50, 3141–3156, 2020.

Ballarotta, M., Ubelmann, C., Pujol, M.-I., Taburet, G., Fournier, F., Legeais, J.-F., Faugere, Y., Delepoulle, A., Chelton, D., Dibarboure, G., and Picot, N.: On the resolutions of ocean altimetry maps, Ocean Science Discussions, 2019, 1–27, https://doi.org/10.5194/os-2018-156, 2019.

Bendat, J. S. and Piersol, A. G.: Random Data: Analysis and Measurement Procedures (Fourth Edition), Wiley-Interscience, New York, 2010.

Chapron, B., Collard, F., and Ardhuin, F.: Direct measurements of ocean surface velocity from space: Interpretation and validation, Journal of Geophysical Research: Oceans, 110, 2005.

Cunningham, H. J., Higgins, C., and van den Bremer, T. S.: The Role of the Unsteady Surface Wave-Driven Ekman–Stokes Flow in the Accumulation of Floating Marine Litter, Journal of Geophysical Research: Oceans, 127, e2021JC018 106, https://doi.org/https://doi.org/10.1029/2021JC018106, e2021JC018106 2021JC018106, 2022.

D'Asaro, E. A.: The energy flux from the wind to near-inertial motions in the surface mixed layer, Journal of Physical Oceanography, 15, 1043–1059, 1985.

Elipot, S. and Gille, S. T.: Ekman layers in the Southern Ocean: spectral models and observations, vertical viscosity and boundary layer depth, Ocean Science, 5, 115–139, https://doi.org/10.5194/os-5-115-2009, 2009.

Elipot, S., Lumpkin, R., Perez, R. C., Lilly, J. M., Early, J. J., and Sykulski, A. M.: A global surface drifter data set at hourly resolution, Journal of Geophysical Research: Oceans, 121, 2937–2966, https://doi.org/10.1002/2016JC011716, 2016.

Flexas, M. M., Thompson, A. F., Torres, H. S., Klein, P., Farrar, J. T., Zhang, H., and Menemenlis, D.: Global Estimates of the Energy Transfer From the Wind to the Ocean, With Emphasis on Near-Inertial Oscillations, Journal of Geophysical Research: Oceans, 124, 5723–5746, https://doi.org/https://doi.org/10.1029/2018JC014453, 2019.

Gill, A. E.: Atmosphere - Ocean Dynamics, Academic Press, San Diego, California, 1982.

GlobCurrent: 1992-Jan-01 to Present, https://doi.org/10.48670/mds-00327.

Hersbach, H., B. B. B. P. B. G. H. A. M. S. J. N. J. P. C. R. R. R. I. S. D. S. A. S. C. D. D. T. J.-N.: Copernicus Climate Change Service (C3S) Climate Data Store (CDS), https://doi.org/10.24381/cds.adbb2d47, 2018.

Higgins, C., Vanneste, J., and van den Bremer, T. S.: Unsteady Ekman-Stokes Dynamics: Implications for Surface Wave-Induced Drift of Floating Marine Litter, Geophysical Research Letters, 47, e2020GL089 189, https://doi.org/https://doi.org/10.1029/2020GL089189, e2020GL089189 10.1029/2020GL089189, 2020.

Klenz, T., Simmons, H. L., Centurioni, L., Lilly, J. M., Early, J. J., and Hormann, V.: Estimates of Near-Inertial Wind Power Input Using Novel In Situ Wind Measurements from Minimet Surface Drifters in the Iceland Basin, Journal of Physical Oceanography, 52, 2417–2430, https://doi.org/10.1175/JPO-D-21-0283.1, 2022.

Lagerloef, G. S. E., Mitchum, G. T., Lukas, R. B., and Niiler, P. P.: Tropical Pacific near-surface currents estimated from altimeter, wind, and drifter data, , 104, 23,313–23,326, https://doi.org/10.1029/1999JC900197, 1999.

Lilly, J. M. and Elipot, S.: A Unifying Perspective on Transfer Function Solutions to the Unsteady Ekman Problem, Fluids, 6, https://doi.org/10.3390/fluids6020085, 2021.

OSCAR: 1992-Jan-01 to Present, https://doi.org/10.5067/OSCAR-03D01.

https://doi.org/10.5194/egusphere-2025-1149
Preprint. Discussion started: 25 March 2025

Plueddemann, A. J. and Farrar, J. T.: Observations and models of the energy flux from the wind to mixed-layer inertial currents, Deep Sea Res. II, 53, 5–30, 2006.

Renault, L., Molemaker, M., McWilliams, J., Shchepetkin, A., Lemarié, F., Chelton, D., Illig, S., and Hall, A.: Modulation of Wind Work by Oceanic Current Interaction with the Atmosphere, Journal of Physical Oceanography, 46, 1685 – 1704, https://doi.org/10.1175/JPO-D-15-0232.1, 2016.

Rio, M.-H., Mulet, S., and Picot, N.: Beyond GOCE for the ocean circulation estimate: Synergetic use of altimetry, gravimetry, and in situ data provides new insight into geostrophic and Ekman currents, Geophysical Research Letters, 41, 8918–8925, https://doi.org/10.1002/2014GL061773, 2014.

Rodríguez, E., Bourassa, M., Chelton, D., Farrar, J. T., Long, D., Perkovic-Martin, D., and Samelson, R.: The Winds and Currents Mission Concept, Frontiers in Marine Science, 6, 438, https://doi.org/10.3389/fmars.2019.00438, 2019.

Shrira, V. I. and Almelah, R. B.: Upper-ocean Ekman current dynamics: a new perspective, Journal of Fluid Mechanics, 887, A24, https://doi.org/10.1017/jfm.2019.1059, 2020.

Taburet, G., Sanchez-Roman, A., Ballarotta, M., Pujol, M.-I., Legeais, J.-F., Fournier, F., Faugere, Y., and Dibarboure, G.: DUACS DT2018: 25 years of reprocessed sea level altimetry products, Ocean Science, 15, 1207–1224, https://doi.org/10.5194/os-15-1207-2019, 2019.

Young, W. and Jelloul, M. B.: Propagation of near-inertial oscillations through a geostrophic flow, Journal of marine research, 55, 735–766, 1997.